Supplementary Information:

Investigating the optimal size of anticancer nanomedicine

Li Tang[a], Xujuan Yang[b], Qian Yin[a], Kaimin Cai[a], Hua Wang[a], Isthier Chaudhury[a], Catherine Yao[a], Qin Zhou[c], Mincheol Kwon[a], James A. Hartman[b], Iwona T. Dobrucki[d], Lawrence W. Dobrucki[e], Luke B. Borst[f], Stéphane Lezmi[g], William G. Helferich[b,1], Andrew L. Ferguson[a,1], Timothy M. Fan[h,1] and Jianjun Cheng[a,e,1]

[a]Department of Materials Science and Engineering, [b]Food Science and Human Nutrition, [e]Bioengineering, [g]Pathobiology and [h]Veterinary Clinical Medicine, and [d]Beckman Institute for Advanced Science and Technology, University of Illinois at Urbana−Champaign, Urbana, Illinois, 61801; [c]Department of Pharmaceutical Science, Guangdong Pharmaceutical College, Guangzhou, Guangdong, 510006, China; [f]Department of Population Health and Pathobiology, North Carolina State University, Raleigh, North Carolina 27606

[1]To whom correspondence may be addressed. E-mail: jianjunc@illinois.edu; t-fan@illinois.edu; alf@illinois.edu; helferic@illinois.edu

Table of contents

General

Materials. All the chemicals including tetraethyl orthosilicate (TEOS, 99.999%) were purchased from Sigma-Aldrich (St Louis, MO, USA) unless otherwise noted. Methoxy-polyethylene glycol$_{5k}$-triethoxysilane (mPEG$_{5k}$-sil) (Fig. 1*A*) was purchased from Laysan Bio (Arab, AL, USA). (S)-2,2',2",2"'-(2-(4-isothiocyanatobenzyl)-1,4,7,10-tetraazacyclododecane-1,4,7,10-tetrayl)tetraacetic acid (*p*-SCN-Bn-DOTA) was purchased from Macrocyclics, Inc. (Dallas, TX, USA). All anhydrous solvents were purified by passing through dry alumina columns and kept anhydrous using molecular sieves. Camptothecin-containing silane (Cpt-NH-sil) (Fig. 1*A*) and Rhodamine B isothiocyanate (RITC)-containing silane (RITC-sil) were prepared as described previously (1). Matrigel™ was obtained from BD Biosciences (Franklin Lakes, NJ, USA). D-luciferin potassium was purchased from Regis Technologies (Morton Grove, IL, USA).

Instrumentation. The sizes and monodispersities of silica nanoparticles (NPs) were determined with a Hitachi S4800 high resolution Scanning Electron Microscope (SEM) and dynamic light-scattering (DLS) instrument. DLS measurement was performed with a 90Plus Particle Size Analyzer (15 mW laser, incident beam = 676 nm, Brookhaven Instruments, Holtsville, NY, USA). ξ-potential was measured with a Malvern Zetasizer Nano-ZS with a 633 nm laser (Malvern Instruments Ltd., Worcestershire, UK). Thermogravimetric Analysis (TGA) was conducted with a Q50 TGA Analyzer (TA Instruments, New Castle, DE, USA). HPLC analyses were performed on a System Gold system (Beckman Coulter, Fullerton, CA, USA) equipped with a 126P solvent module, a System Gold 128 UV detector and an analytical C18 column (Luna C18, 250 × 4.6 mm, 5 μm, Phenomenex, Torrance, CA, USA).

Cell culture. MCF-7 cells were obtained from ATCC (Manassas, VA, USA). Murine 4T1 cells engineered with firefly luciferase were provided by Dr. David Piwnica-Worms from Washington University (St. Louis, MO, USA). Cells were cultured in DMEM medium containing 10% fetal bovine serum (FBS), 100 units/mL aqueous Penicillin G and 100 μg/mL streptomycin (Invitrogen, Carlsbad, CA, USA) at 37 °C in 5% CO_2 humidified air. For the culture of MCF-7 cells, 1 nM estrogen (Sigma-Aldrich Inc., St. Louis, MO, USA) was added to the cell media. The absorbance wavelength on a microplate reader (Perkin Elmer, Victor$^3{}_{TM}$ V, Waltham, MA, USA) was set at 570 nm for MTT assay. The confocal microscopy images for cellular internalization

tumor penetration studies were taken on a Zeiss LSM700 Confocal Microscope (Carl Zeiss, Thornwood, NY, USA) using a 63×/1.4 oil lens with excitation wavelength set at 405, 488 and 555 nm.

Animals. Female athymic nude mice were purchased from the National Cancer Institute (NCI, Frederick, MD, USA) and ovariectomized at the age of 21 days by the vendor. After arrival, mice were single-cage housed and had free access to food and water. Female BABL/c mice were purchased from NCI. Female C57BL/6 mice were purchased from Charles River (Wilmington, MA, USA) for pharmacokinetics study. Feed and water were available *ad libitum*. Artificial light was provided in a 12/12 hour cycle. The study protocol was reviewed and approved by The Illinois Institutional Animal Care and Use Committee (IACUC) of the University of Illinois at Urbana Champaign.

Preparation and characterization of size-controlled silica NCs

Preparation of camptothecin-silica nanoconjugates (Cpt-NCs) of controlled sizes. Cpt-NCs of 200, 50 and 20 nm in diameter (denoted as Cpt-NC200, Cpt-NC50 and Cpt-NC20, respectively) were prepared as previously reported (1) and used for all reported efficacy studies. Briefly, the silica cores with controlled sizes were first prepared using Stöber method. To prepare 200-nm NPs, methanol (1 mL), DI water (0.27 mL) and concentrated ammonia (0.24 mL) were mixed. Then TEOS (62.5 μL) was added to the mixture. The solution was stirred gently for 24 h at room temperature. The NPs were collected by centrifugation at 15k rpm and washed with ethanol (1 mL × 3). Synthetic procedures were similar for silica NPs of other sizes, except for the amount of reagents used (1). Cpt-NH-sil was synthesized as previously reported (1). To prepare Cpt-NCs of 200, 50 or 20 nm, silica NP prepared with the corresponding, desired size as described above (4.1 mg) was redispersed in a mixture of MeOH (0.7 mL) and DI water (0.2 mL) followed by the addition of Cpt-NH-sil (1.7 mg) in DMSO (100 μL). After the mixture was stirred for 10 min and homogenized, a NaF aqueous solution (25 μL, 10 mg/mL) was added. The supernatant of the mixture was monitored by HPLC to quantify the unreacted Cpt species in order to determine the incorporation efficiency of Cpt to NCs. Drug loadings were calculated based on the feeding ratio

of drugs and incorporation efficiency with the assumption that TEOS was completely hydrolyzed. After reaction, without isolation of the Cpt-NCs, surface modification was carried out by the addition of a methanol solution of $mPEG_{5k}$-sil (10 mg/mL) at the weight ratio of $mPEG_{5k}$-sil/NC of 0.05, 0.1, 0.2 for Cpt-NCs of 200, 50 and 20 nm, respectively. The mixture was stirred for another 12 h at room temperature. Surface modified NCs were collected by centrifugation at 15k rpm and the supernatant was removed. The isolated NCs were washed with ethanol (1 mL × 3) and redispersed in DI water or PBS (1×) before use. The NC sizes were characterized by SEM and DLS.

Preparation of rhodamine labelled silica NCs (Rhd-NCs) of controlled sizes. Rhd-NCs of varying sizes (Rhd-NC200, Rhd-NC50 and Rhd-NC20) were prepared as previously reported (1) for the cellular internalization and tumor penetration studies.

Preparation of PEGylated blank silica NCs of controlled sizes. Blank silica NCs without drug were prepared similarly as described above using Stöber method (2). After reaction, without isolating the silica NCs, surface modification was carried out by directly adding a methanol solution of $mPEG_{5k}$-sil (10 mg/mL) at the weight ratio of $mPEG_{5k}$-sil/NC=0.05, 0.1, 0.2 for NCs of 200, 50 and 20 nm respectively. The mixture was stirred for another 12 h at rt. Surface modified NCs were collected, washed and redispersed in PBS (1×) before use. These PEGylated blank silica NCs of three different sizes (denoted as NC200, NC50 and NC20) were used for TGA analysis to determine the PEG density and as control NCs in efficacy studies.

Preparation of DOTA conjugated silica NCs (DOTA-NCs) of controlled sizes. DOTA-NCs of varying sizes were prepared as previously reported (3) for the biodistribution and pharmacokinetics studies. Briefly, silica NPs of controlled sizes were first prepared using Stöber method. DOTA containing silane (DOTA-sil) was synthesized as previously reported (3). Next, without isolating the silica NCs, a methanol solution (200 μL) of DOTA-sil (2 mg, 2.6 μmol) was added to the reaction mixture and stirred for 10 min followed by the addition of $mPEG_{5k}$-sil (10 mg/mL) to modify the surface of NCs. The resulting NCs were collected, washed and redispersed in DI water or PBS (1×) before use.

^{64}Cu labelling of DOTA-NCs. The ^{64}Cu chloride (Washington University in at St. Louis, MO, USA) was mixed with DOTA-NCs (2 mg) in NH_4OAc buffer (pH = 5.5, 0.1 M, 0.3 mL). The

mixture was incubated for 1 h at 80 °C. To determine the labelling efficiency, the NCs were centrifuged down (15k rpm, 5 min) and the radioactivity in the supernatant and the precipitation was measured respectively. The ^{64}Cu-labeled silica NCs were purified by centrifugation and washed by PBS (1×) (1 mL × 1). The purified ^{64}Cu-labeled silica NCs of different sizes (^{64}Cu-NC200, ^{64}Cu-NC50 and ^{64}Cu-NC20) were then re-suspended in PBS (1×) for intravenous (iv) injection. Stability of ^{64}Cu labeling with ^{64}Cu-NCs was investigated similarly as previously reported in 50% reconstituted human serum (Sigma-Aldrich, 0.6 mg/mL) at 37 °C for 48 h (3).

DLS and ξ-potential measurements. The hydrodynamic size was measured with 90Plus Particle Size Analyzer by dispersing the PEGylated NCs in PBS (1×) at concentration of 0.5 mg/mL. Measurements were taken at a 90° scattering angle. The ξ-potential of the NCs was determined with a Malvern Zetasizer. The freshly prepared PEGylated NCs were dispersed in DI water to a concentration of 0.5 mg/mL.

TGA measurements and surface PEG density. PEGylated blank silica NCs were dried at 60 °C under vacuum overnight before the TGA analysis. Dried, PEGylated NCs of 200, 50 or 20 nm (~2-3 mg) were loaded to sample cups. Thermogravimetric analysis was performed on Q50 TGA Analyzer under nitrogen and oxygen (50/50%) flow at a heating rate of 10 °C min^{-1} (rt to 800 °C). The loss of organic species at 200-600 °C range in TGA curves was calculated to determine the weight percentage of PEG on the surface of silica NCs. The number of PEG molecules per nm2 was calculated based on wt% of PEG per NC and its surface area. Silica NC density was set as 2.56 g/cm^3. The average size determined by SEM was used as NC diameter

Release kinetics of Cpt from Cpt-NCs. The Cpt-NCs (Cpt-NC200, Cpt-NC50 or Cpt-NC20) were dispersed in 50% reconstituted human serum (0.6 mg/mL), equally distributed to 20 vials with 1 mL NC solution per vial, and then incubated at 37°C. At selected time intervals, three vials of each group were taken out of the incubator. The NC solution was mixed with equal volume of methanol (1 mL) and centrifuged at 15,000 rpm for 10 min. The supernatant (1 mL) was transferred to an Eppendorf tube without disturbing the precipitates (NCs) and tuned to pH 2 with phosphoric acid (85%, 100 μL). The resulting solution was directly injected into HPLC equipped with an analytical C18 column. A mixture of acetonitrile and water (containing 0.1% TFA) at a volume ratio of 1:3 was used as the mobile phase. The flow rate was set at 1 mL/min.

The area of the HPLC peak of the released Cpt (λ_{abs} = 370 nm) was intergraded for the quantification of Cpt as compared to a standard curve of free Cpt prepared separately. The Cpt release kinetic profiles were showed in Fig. S1*B*.

Stability of PEGylated silica NCs in cell medium containing 10% FBS. PEGylated silica NCs (1.5 mg) were dispersed in 2 mL cell medium containing 10% FBS at 37 °C. The hydrodynamic diameter (which is ~30-50 nm larger than the diameter of hard cores of NCs measured by SEM) of NCs were monitored by DLS and followed for 24 h.

Pharmacokinetics study. To evaluate the circulation half-life of silica NCs, ^{64}Cu labelled DOTA-NCs of different sizes (^{64}Cu-NC200, ^{64}Cu-NC50 and ^{64}Cu-NC20) were injected iv into female C57BL/6 mice (n = 3) through tail veins (~40 μCi per mouse). Blood (20-50 μL) was collected through orbital sinus at 3 min, 30 min, 1 h, 3 h, 5 h, 12 h, 24 h post injection (p.i.). The collected blood was weighed and subjected for the measurement of radio activity (^{64}Cu) with Wizard2 γ-counter (Perkin-Elmer, USA). Activity in each collected sample was calculated as percentage of injected dose per gram of blood (%I.D./g). For this calculation, the radio activity in tissue was corrected for decay to the time of γ-well counting. The blood half-life was determined by the following equation (4):

$$\text{Blood half-life} = \frac{\ln 2 \times time_{interval}}{\ln(concentration_{peak} / concentration_{trough})} \quad (1)$$

where time interval is the time between the peak and the end point. Concentration peak is the maximum concentration in blood (3 min p.i.) and the concentration trough is the concentration at the end point (24 h p.i.).

A

Name of NC	DLS[a]		wt% of PEG[b]	ζ-potential (mV)	I.E.[c] (%)	LD[d] (wt%)
	D ± SD (nm)	PDI ± SD				
Cpt-NC200	238.0 ± 3.3	0.058 ± 0.023	2.3	-0.70	81.0	16.2
Cpt-NC50	65.2 ± 0.4	0.090 ± 0.031	9.3	-0.38	83.2	16.6
Cpt-NC20	43.8 ± 0.3	0.121 ± 0.017	18.0	-3.89	79.3	15.9

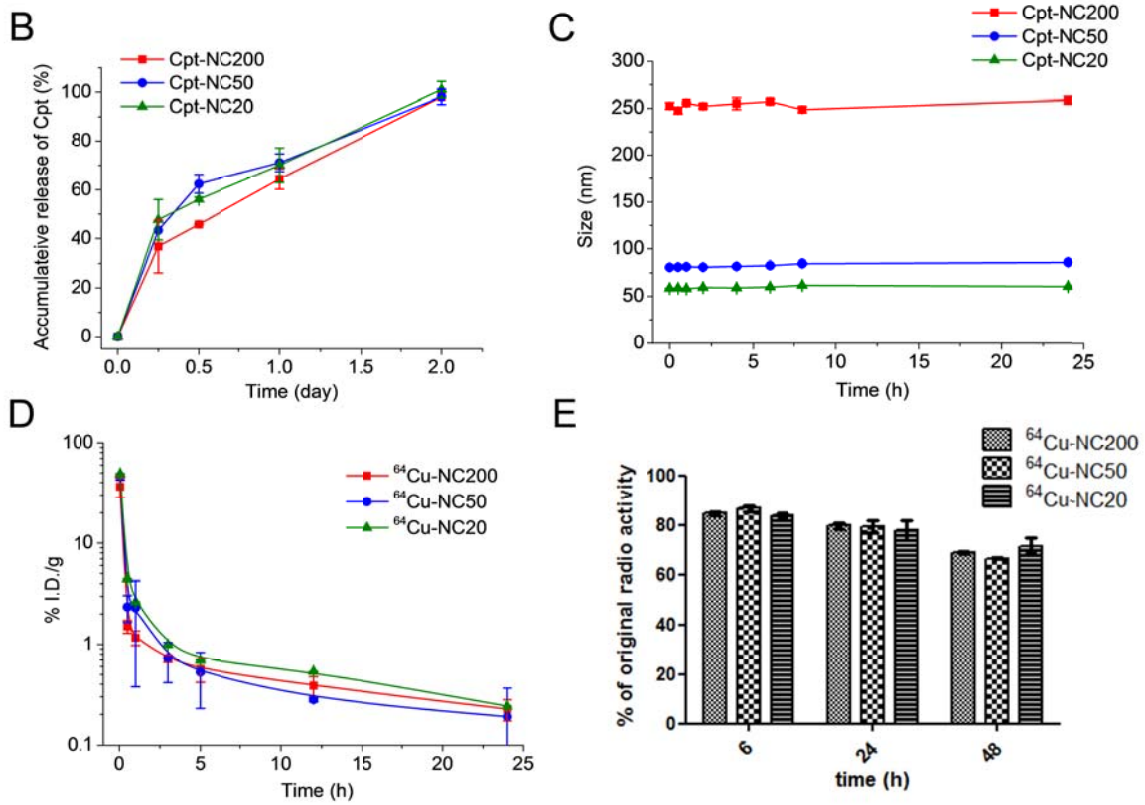

Fig. S1. Characterizations of silica NCs. (*A*) Characterization of the size-controlled Cpt-NCs. [a] The hydrodynamic sizes and polydispersity (PDI) were measured by dynamic light scattering (DLS); [b] Weight percentage (wt%) of PEG_{5k} per NC was determined by TGA; [c] The incorporation efficiency (I.E.) was determined by monitoring and quantifying the concentration of free Cpt in the supernatant using HPLC by centrifuging down the NCs; [d] drug loading (LD) was determined by HPLC. (*B*) Release kinetics of Cpt from Cpt-NCs of different sizes in 50% reconstituted human serum. (*C*) PEGylated Cpt-NCs are stable in cell medium containing 10% FBS. (*D*) Blood clearances of silica NCs of different sizes follow similar trends. (*E*) Stability of ^{64}Cu labeling with ^{64}Cu-NCs in 50% reconstituted human serum at 37 °C.

Size dependent biodistribution, tumor penetration and clearance, and cellular internalization studies

In vivo biodistribution study in MCF-7 xenograft human breast tumor model. Athymic nude mice bearing MCF-7 tumors (size: ~7 mm × 7 mm) were divided into groups of five, minimizing tumor size variations between groups. Mice were injected iv with ^{64}Cu labelled silica NCs, 200, 50 or 20 nm in diameter (denoted as ^{64}Cu-NC200, ^{64}Cu-NC50 and ^{64}Cu-NC20 respectively; each mouse received ~50 μCi radioactivity). Micro-PET/CT imaging of animals was performed with small animal dedicated Siemens Inveon PET-CT system (Siemens Healthcare, USA). Mice were anesthetized with isoflurane (1-3 %) and placed on the imaging bed and kept in the same isoflurane flow. A dynamic PET scan was acquired for 1 h (60 min acquisition time, reconstructed as 60 frames at 60 seconds/frame). The micro-CT scan (80keV/500uA X-rays energy, 360 projections, 360 degrees, pixel size: 75 μm) was used for determining the anatomical localization of tumors. Static micro-PET scans were acquired at selected time points (3, 6, 24 and 48 h p.i.) together with micro-CT scans for anatomical co-registration. The obtained micro-PET and micro-CT images were reconstructed using ordered subset expectation maximization (OSEM) and cone-beam algorithms with existing commercial software (Inveon Acquisition Workspace and Cobra Exxim, respectively). Micro-PET images were processed using 3-D median filtering and fused with micro-CT images. To quantify the radioactivity of ^{64}Cu in tumors, complex irregular volumes of interest (VOIs) were drawn on the micro-CT images and registered with the micro-PET images to determine mean counts in each VOI. To minimize partial volume effects, the anatomical borders of the organs were not included. The radiotracer activity from each VOI was normalized by injected dose and expressed as per cent of the decay-corrected injected activity per cm^3 of tissue, which can be approximated as %I.D./g assuming the

density of tissue is ~1.0 g/cm^3. The initial total injected activity was determined by dose calibrator before the injection.

Radioactivity measurement with γ-counter. *Ex vivo* measurement of the radio activity was conducted withWizard2 Automatic γ-counter (Perkin-Elmer, USA). Mice were euthanized and dissected after the final micro-PET/CT imaging session (24 h p.i.). All the major organs were collected, weighed and measured for radio activity (^{64}Cu) with γ-counter using appropriate energy window centered at photopeak of 511 keV. Raw counts were corrected for background, decay, and weight. Corrected counts were converted to micro-curie (μCi) per gram by use of a previously determined calibration curve by counting ^{64}Cu standards. Activity in each collected tissue sample was calculated as percentage of injected dose per gram of tissue (%I.D./g). For this calculation, the radio activity in tissue was corrected for decay to the time of γ-well counting. Data are presented as %I.D./g (average ± SEM). The statistical analysis was performed using a two-tailed Student's t-test, and *p*-values < 0.05 were considered statistically significant.

Cellular internalization of silica NCs of different sizes in MCF-7 cells. In the qualitative analysis by confocal laser scanning microscopy, MCF-7 cells (5×10^4) were seeded in a 4-well chamber slide for 24 h. Cells were washed once with opti-MEM and then incubated for 1 h (37 °C) with opti-MEM (1 mL) containing 100 μg/mL Rhd- NCs (Rhd-NC200, Rhd-NC50 and Rhd-NC20). The cells were then washed by PBS (1×) (1 mL) for three times. Cells were then fixed with 4% paraformaldehyde and subsequently imaged by confocal laser scanning microscopy. The cell nucleus was stained with 4',6-diamidino-2-phenylindole (DAPI) and cell actins were stained with phalloidin-Alexa Fluo488.

Ex vivo tumor penetration study in MCF-7 tumors. MCF-7 tumors (size: ~7.0 × 7.0 mm, n = 3) were *ex vivo* cultured with Rhd-NC200, Rhd-NC50 or Rhd-NC20 in cell culture medium at 37 °C for 48 h (Fig. S4). Tumors without any treatment served as the control. The flash frozen tumor tissues were embedded with optimum cutting temperature compound (OCT) (Sakura Finetek USA, Torrance, CA, USA). Tumor sections (7 μm thickness) were collected by cryostat with a Leica CM3050S cryostat and mounted on glass slides. Fluorescent images were taken on a Zeiss Axiovert 200M fluorescence microscope. A tiling image was taken with fixed exposure time to show the NC penetration in tumor sections. The fluorescence intensity in tumor sections

was analyzed by ImageJ. To quantify the penetration of NCs, we defined the tumor tissue penetration depth as the distance from the periphery of the tumor to the site where the fluorescence intensity decreased by 95% as compared to the fluorescent intensity at the tumor periphery.

In vivo tumor penetration study in athymic nude mice bearing MCF-7 tumors. Athymic nude mice bearing MCF-7 tumors (size: ~7.0 × 7.0 mm) were divided into groups of three. Mice were injected iv with PBS or Rhd-NC200, Rhd-NC50 and Rhd-NC20 (200 μL, 15 mg/mL). The animals were euthanized 3 h after administration. The tumors were collected and immediately frozen in OCT and further sectioned at 7 μm thickness in a cryostat for immunohistochemical staining. The slides were incubated with CD31 antibody (1/100) at 4 °C overnight and then stained with a FITC-conjugated secondary antibody (1/150) at 37 °C for 1 h in the dark. The nucleus was stained with DAPI. Fluorescence images were taken on a Zeiss LSM 700 confocal microscope. FITC fluorescence representing endothelial cells was visualized using 488 nm laser excitation. Red fluorescence of rhodamine, representing silica NCs, was visualized with 555 nm laser excitation.

Ex vivo tumor clearance study in MCF-7 and 4T1 tumors. MCF-7 tumors (size: ~7.0 × 7.0 mm, n = 3) were *ex vivo* cultured with Rhd-NC50 or Rhd-NC20 in opti-MEM at 37 °C for 24 h. The tumors were then washed with PBS (2 mL × 3) and immerged in fresh opti-MEM of same volume (replaced by fresh opti-MEM every 12 h for 48 h) (Fig. S6). The fluorescence intensity in the original opti-MEM solution containing Rhd-NC50 or Rhd-NC20 and all the opti-MEM solutions collected at different time points (12, 24, 36, 48 h) were measured with a LS55 fluorescence spectrometer (Perkin Elmer, Santa Clara, CA, USA) to determine the amount of the cleared Rhd-NCs from the tumor tissue. After 48 h, the flash frozen tumor tissues were embedded with OCT and processed similar as above mentioned and then imaged with Zeiss Axiovert 200M fluorescence microscope. The tumor clearance in 4T1 tumors was studied similarly.

Cytotoxicity of Cpt-NCs against MCF-7 and 4T1 cells by MTT assay. MCF-7 cells were seeded in 96-well plates at 3,000 cells/well and grown in culture medium containing 10% FBS at 37 °C for 24 h. The medium was replaced with fresh medium containing Cpt, Cpt-NCs of varying sizes

in concentrations ranging from 1 nM to 10 μM of Cpt or equivalent Cpt. At each concentration, six wells per plate were treated. The cell viability was determined by MTT assay after 72 h. The standard MTT assay protocols were followed thereafter(5). Cytotoxicity of Cpt-NCs against 4T1 cells was studied following the same procedures.

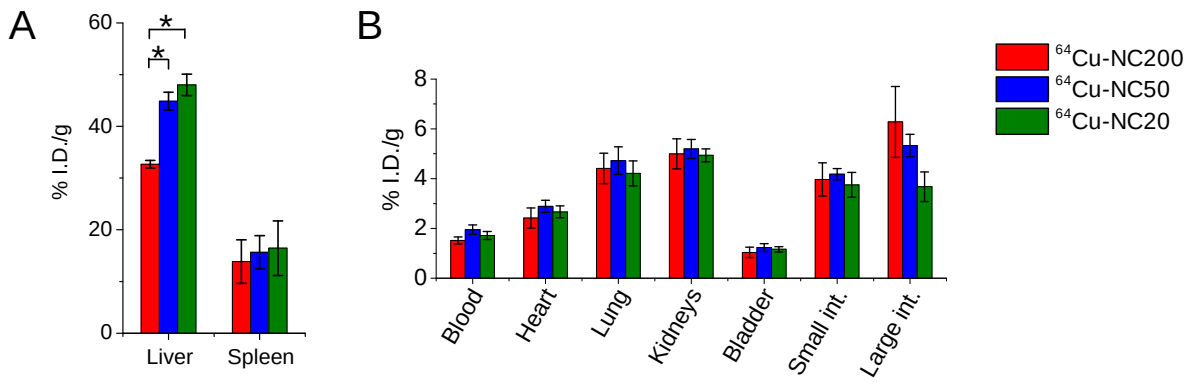

Fig. S2. *In vivo* biodistribution of ^{64}Cu-NCs in athymic nude mice bearing MCF-7 tumors. Athymic nude mice bearing MCF-7 tumors were injected iv with ^{64}Cu-NC200, ^{64}Cu-NC50 and ^{64}Cu-NC20. Mice were euthanized 24 h p.i.. Mouse tissues including liver and spleen (*A*) and blood, heart, lung, kidneys, bladder, small and large intestines (*B*) were collected and measured for radioactivity by γ-counter (average ± SEM; n = 5; two-tailed Student's t-test: $*p < 0.05$).

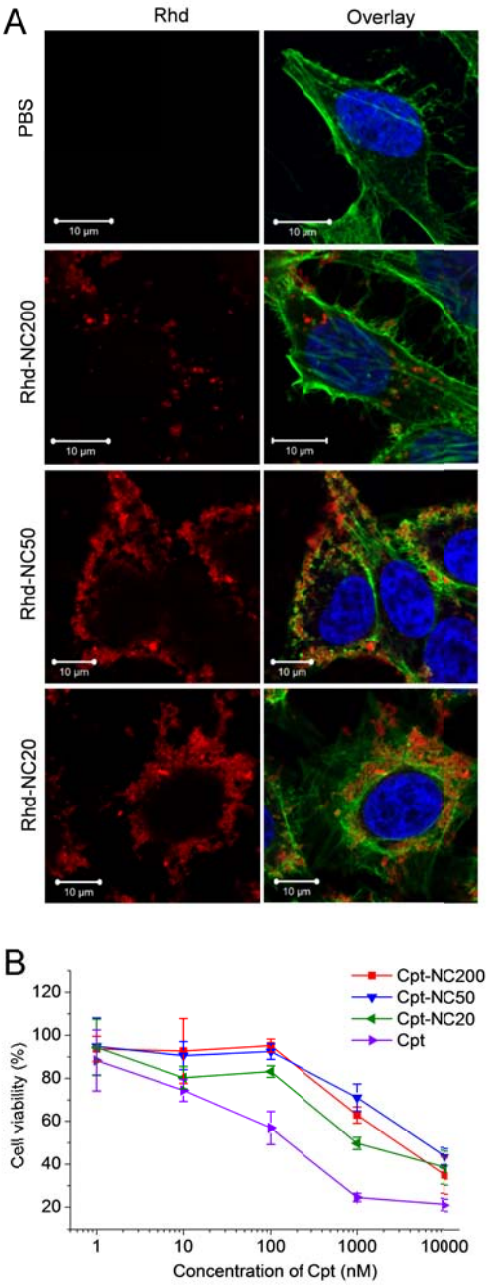

Fig. S3. (*A*) Confocal laser scanning microscopy images of MCF-7 cells after 2 h incubation at 37 °C with Rhd-NC200, Rhd-NC50 or Rhd-NC20 (red). Nuclei were stained by DAPI (blue). Cell actins were stained with phalloidin-Alexa Fluo488 (green). Scale bar: 10 μm. (*B*) *In vitro* cytotoxicity of Cpt-NCs against MCF-7 cells.

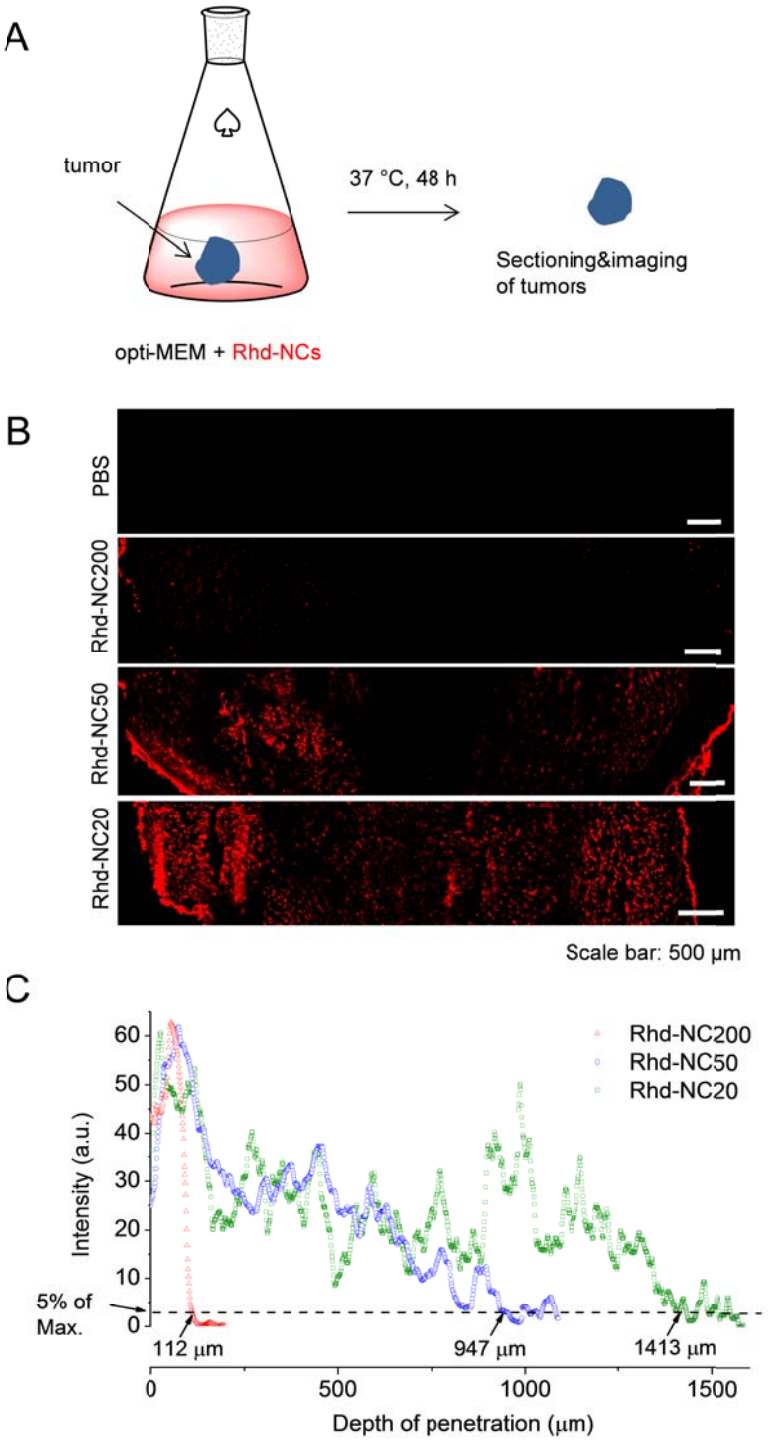

Fig. S4. *Ex vivo* tumor penetration study in MCF-7 tumors. (*A*) Illustration of the experiment procedure. MCF-7 tumors (size: ~7.0 × 7.0 mm, n = 3) were *ex vivo* cultured with Rhd-NCs in

opti-MEM for 48 h. The tumors without any treatment served as the control. The tumor sections of treatment groups (7 μm in thickness) were collected by cryostat, mounted on glass slides and analyzed on a fluorescence microscope. (*B*) A tiling image was taken with fixed exposure time to show the NC (red) penetration in tumor sections. Scale bar = 500 μm. (*C*) To quantify the penetration depth, we defined the tumor tissue penetration depth as the distance from the periphery of the tumor to the site where the fluorescence intensity decreases by 95% as compared to the fluorescent intensity at tumor periphery. The penetration depths of Rhd-NC200, Rhd-NC50 and Rhd-NC20 were found to be 112 μm, 947 μm and 1413 μm, respectively.

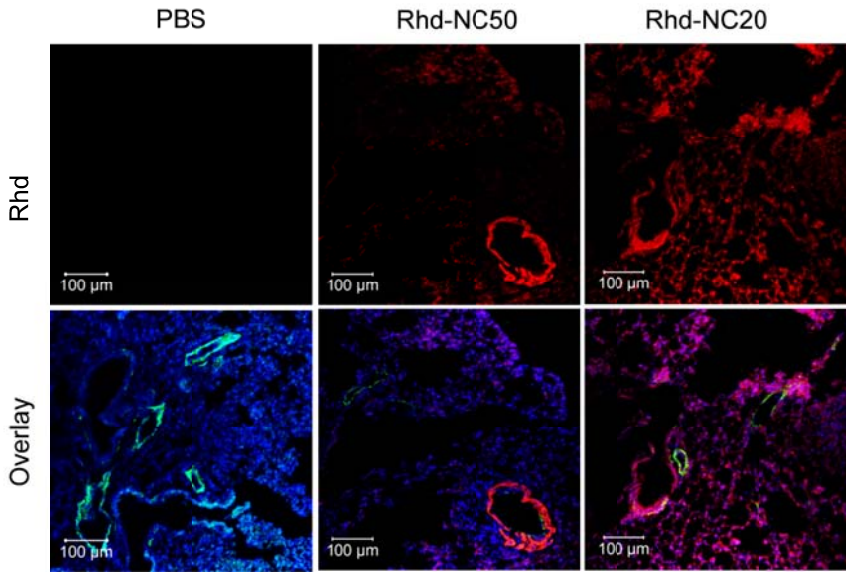

Fig. S5. *In vivo* tumor penetration study in athymic nude mice bearing MCF-7 tumors. Athymic nude mice bearing MCF-7 tumors (size: ~7.0 × 7.0 mm , n = 3) were injected iv with Rhd-NC50, Rhd-NC20 or PBS as control. Mice were euthanized 3 h p.i.. The tumors were collected, flash frozen in optimum cutting temperature compound (OCT), sectioned (7 μm in thickness) and stained with CD31 to indicate the blood vessels (green). Representative images show the distribution of Rhd-NCs (red) in the tumor tissues. The nuclei were stained with DAPI (blue).

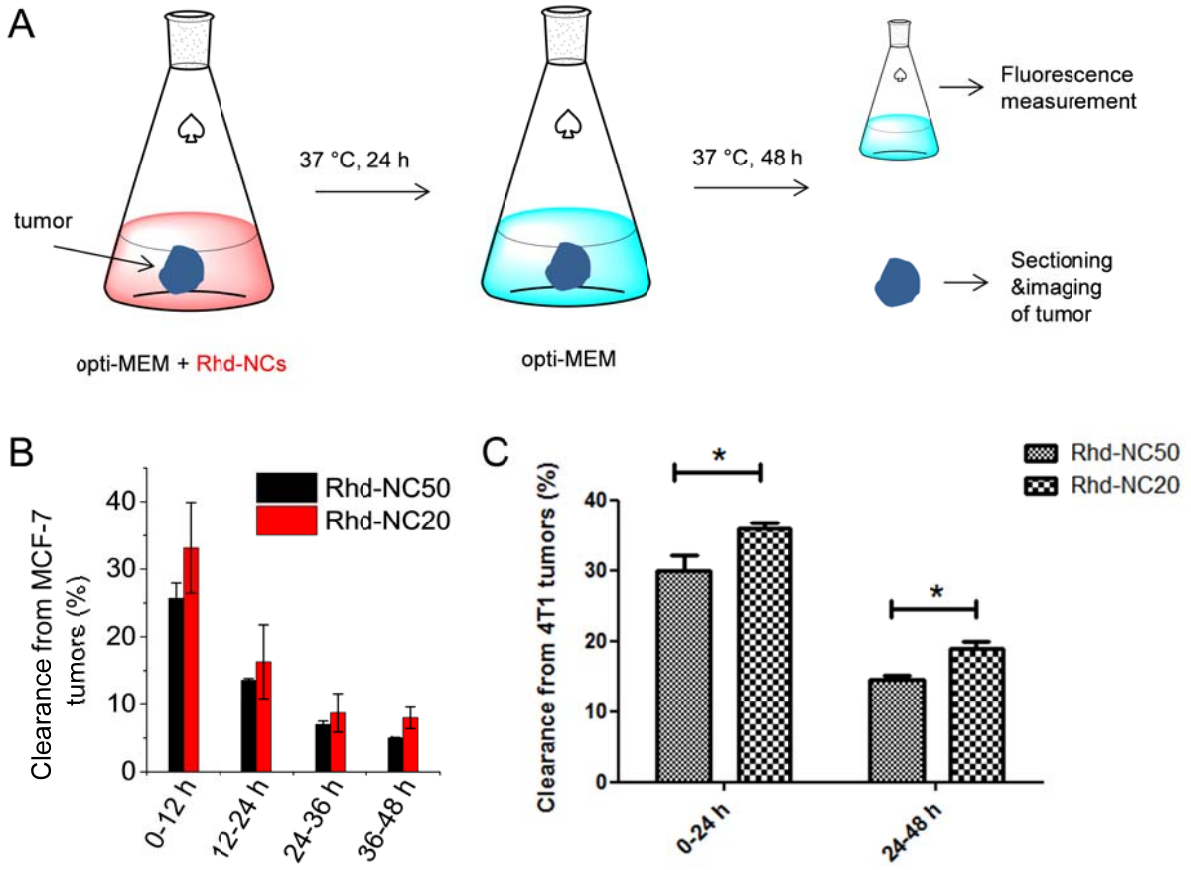

Fig. S6. *Ex vivo* tumor clearance study in MCF-7 and 4T1 tumors. (*A*) Illustration of the experiment procedure. MCF-7 tumors (size: ~7.0 × 7.0 mm, n = 3) were *ex vivo* cultured with Rhd-NCs of different sizes in opti-MEM for 24 h to allow the silica NCs penetrate into the tumors passively. Then the solution was replaced with fresh opti-MEM (change every 12 h until another 48 h) and the tumors were immersed in the fresh media. The fluorescence intensity in the opti-MEM solutions were monitored with fluorescence spectrometer. After 48 h, the tumor sections of treatment groups (7 μm in thickness) were collected by cryostat, mounted on glass slides and analyzed on a fluorescence microscope. (*B*) Monitoring of the fluorescence intensity in the opti-MEM solutions collected at different time points. (*C*) Monitoring the clearance of the Rhd-NCs from the excised 4T1 tumors similarly (size: ~7.0 × 7.0 mm n = 4; average ± SEM; two-tailed Student's t-test: $*p < 0.05$).

In vivo efficacy studies in a primary tumor model

Acute antitumor efficacy study in athymic nude mice bearing subcutaneously implanted MCF-7 human breast tumors. Female athymic nude mice, 8-week old, were prepared for implantation of the tumor cells. MCF-7 cells were collected from culture, and 1×10^6 cells suspended in a 1:1 mixture of Hank's Balanced Salt (HBS) buffer and matrigel were then injected subcutaneously into the flanks of a mouse (four injection sites per mouse). After about 3 weeks when tumors had reached ~50 mm^3, mice were divided into four groups that each had 5-6 mice, minimizing weight and tumor size difference among the groups. Tumor-bearing mice of the corresponding group were treated three times (every four days) through iv injection of PBS (1×, 200 μL), 20 mg Cpt/kg of Cpt-NC200, Cpt-NC50, and Cpt-NC20, respectively. The experimental time line and injection protocol are summarized in Fig. S7. All the mice were sacrificed on Day 12. All the tumors were collected, weighed, imaged with camera and preserved for further analysis. Harvested tumor samples were fixed in 10% formalin and transferred to 70% ethanol after 48 h. Fixed tumors were embedded in paraffin blocks, cut into 5 μm sections and placed on microscopic slides. Cell proliferation index in tumors was determined using immunohistochemical staining for the cell proliferation marker, Ki-67, following the manufacture's procedure. Positive cells were brown. In separate tissue sections, cell apoptosis was analyzed using *in situ* cell death detection kit (Roche Diagnostics GmbH, Mennheim, Germany) and TUNEL staining was performed following the manufacture's procedure. Positive cells were green fluorescent (TUNEL) and background cells were blue fluorescent (4',6-diamidino-2-phenylindole (DAPI)). The tissue sections were observed on a microscope (Zeiss Axiovert 200M) for bright field and fluorescence images. Both the positive and the background cells in tissue sections with Ki-67 or TUNEL staining were counted in the images with ImageJ to determine the proliferation index and apoptosis index. Data are represented as average ± SEM (standard error of the mean) and are analyzed by One-way ANOVA (Fisher) ($0.01 < *p \leq 0.05$; $**p \leq 0.01$) (n=20).

Long term tumor reduction and mouse survival study in athymic nude mice bearing subcutaneously implanted MCF-7 human breast tumors. Female athymic nude mice, 8-week old, were prepared for implantation of the tumor cells. MCF-7 cells were collected from culture, and

1×10^6 cells suspended in a 1:1 mixture of HBS buffer and matrigel were then injected subcutaneously into the flanks of a mouse (four injection sites per mouse). After about 3 weeks when tumors had reached ~50 mm^3, mice were divided into six groups that each had 5-6 mice, minimizing weight and tumor size difference among the groups. Tumor-bearing mice were treated three times (every four days) by iv injection of PBS (1×), PEGylated blank silica NPs (50 nm in diameter, equivalent amount of silica as Cpt-NC200, Cpt-NC50 and Cpt-NC20), Cpt-NC200 (20 mg Cpt/kg), Cpt-NC50 (20 mg Cpt /kg), Cpt-NC20 (20 mg Cpt /kg) and free irinotecan (100 mg/kg) through intraperitoneal (ip) injection every week. Very similar anti-tumor efficacies were reported when irinotecan was administered at the optimal dose by either ip or iv route in various tumor models (6). The experimental time line and injection protocol are summarized in Fig. S7. After dosing, the animals were monitored closely for body weight and food intake. The measurements of the tumor size for each animal were performed at regular intervals using calipers without knowledge of which injection each animal had received. The tumor volume for each time point was calculated according to the formula (length) × $(width)^2/2$. If body weight loss is beyond 20% of predosing weight, the animals were euthanized. When the tumor load reached 400 mm^3 (as predetermined endpoint) or the animal had become moribund, the mouse was sacrificed. When an animal exited the study due to tumor size or treatment related death, the final tumor size recorded for the animal was included with the data used to calculate the mean size at subsequent time point. Curves were truncated after two or more deaths occurred.

The time to endpoint (TTE) for each mouse was calculated from the following equation:

$$TTE(days) = \frac{\log_{10}(endpo\,\mathrm{int}\,volume) - b}{m} \qquad (2)$$

where b is the intercept of the line and m is the slope of the line obtained by linear regression of a log-transformed tumor growth data set comprised of the first observation that exceeded the study endpoint volume and the three consecutive observations that immediately preceded the attainment of the endpoint volume. Animals that do not reach the endpoint are assigned a TTE value equal to the last day of the study (99 days). Animals classified as TR (treatment-related) deaths or NTR (non-treatment-related metastasis) deaths are assigned a TTE value equal to the day of death. Animals classified as NTR (non-treatment-related) deaths are excluded from TTE

calculations. Treatment efficacy was determined from tumor growth delay (TGD), which is defined as the increase in the median time to endpoint (TTE) in a treatment group compared to the control group. The median TTE of each group is the basis for determining treatment efficacy. TGD is calculated as the difference between the median TTE for a treatment group and the median TTE of the control group:

$$TGD = T - C \tag{3}$$

expressed in days, or as a percentage of the median TTE of the control group:

$$\%TGD = \frac{T - C}{C} \times 100\% \tag{4}$$

Where T is the median TTE for a treatment group, C is the median TTE for the control Group (PBS group). All statistical data analysis was conducted using OriginPro® 8.5 (OriginLab Corporation, Northampton, MA, USA) program. Data of tumor size measured on the same time point were analyzed using one-way ANOVA (OriginPro) with post hoc Fisher's LSD test.

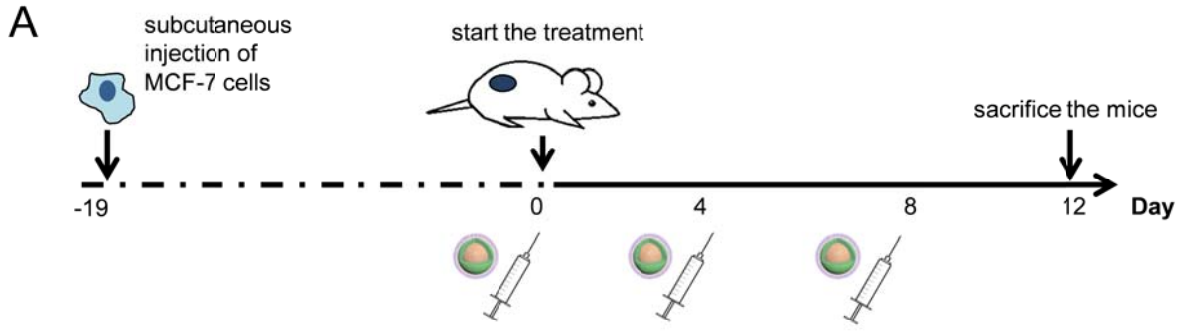

B

Group description	Mice #	Dose of drug equiv.	Injection route	Schedule
PBS	5	0	iv	Q4d × 3
Cpt-NC200	5	20 mg/kg	iv	Q4d × 3
Cpt-NC50	5	20 mg/kg	iv	Q4d × 3
Cpt-NC20	5	20 mg/kg	iv	Q4d × 3

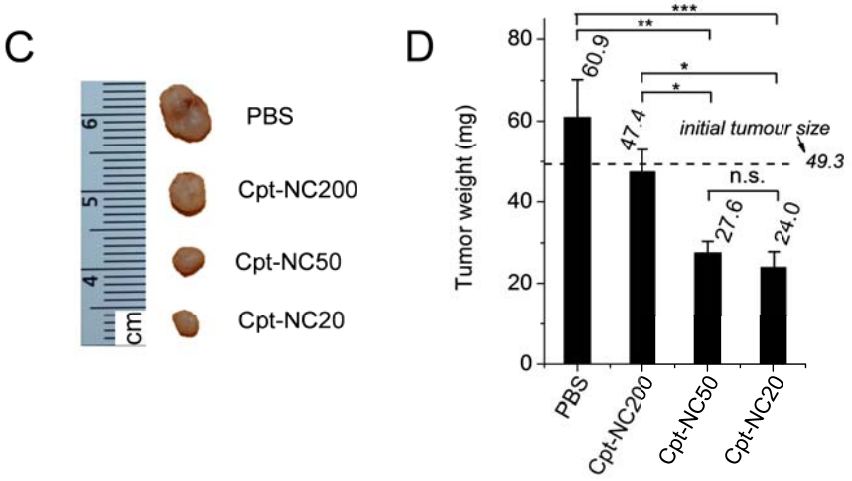

Fig. S7. Acute antitumor efficacy study in athymic nude mice bearing subcutaneously implanted MCF-7 tumors. (*A*) Schematic illustration of the time line of the efficacy study. (*B*) Injection protocol of all the treatment groups. The first dose was administered on day 0 for all groups; Q4d × 3, three injections with 4 day intervals. (*C*) Representative pictures of MCF-7 tumors which were collected after the mice were sacrificed at Day 12. (*D*) All the MCF-7 tumors (n = 20) were collected and weighed after the mice were sacrificed.

A

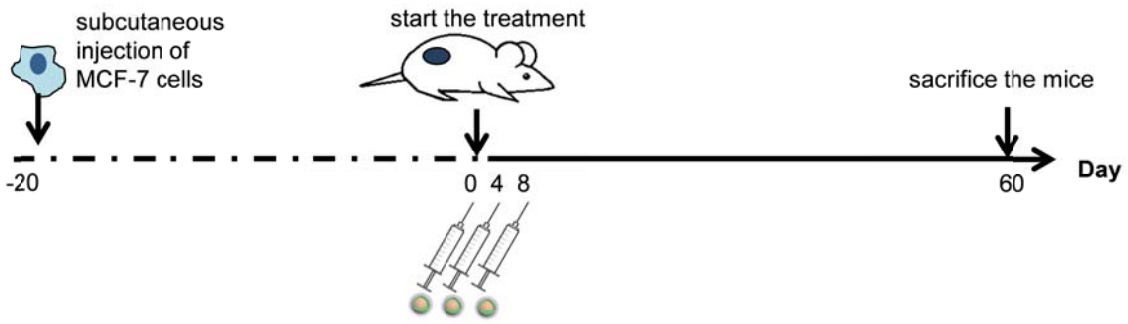

B

Group	Mice #	Dose of Cpt equiv.	Injection route	Schedule [a]	N_{TR}[b]	N_{NTR}[c]	N_{EU}[d]
PBS	5	0	iv	Q4d × 3	0	0	5
Blank NP	5	0	iv	Q4d × 3	0	0	5
Irinotecon	5	100 mg/kg	ip	Qwk × 3	0	0	0
Cpt-NC200	5	20 mg/kg	iv	Q4d × 3	0	0	5
Cpt-NC50	5	20 mg/kg	iv	Q4d × 3	0	0	1
Cpt-NC20	5	20 mg/kg	iv	Q4d × 3	0	1	3

C

Group A (Vs.) Group B	Days post injection					
	0	6	8	18	30	40
Blank NP PBS	n.s.	n.s.	*	n.s.	n.s.	n.s.
Irinotecan PBS	n.s.	n.s.	***	***	***	***
Cpt-NC200 PBS	n.s.	n.s.	**	**	***	***
Cpt-NC50 PBS	n.s.	*	***	***	***	***
Cpt-NC20 PBS	n.s.	n.s.	***	***	***	***
Irinotecan Blank NP	n.s.	n.s.	*	***	***	***
Cpt-NC200 Blank NP	n.s.	n.s.	n.s.	***	***	***
Cpt-NC50 Blank NP	n.s.	**	**	***	***	***
Cpt-NC20 Blank NP	n.s.	*.	n.s.	***	***	***
Cpt-NC50 Cpt-NC200	n.s.	*	*	**	*	**
Cpt-NC20 Cpt-NC200	n.s.	n.s.	n.s.	*	*	n.s.
Cpt-NC20 Cpt-NC50	n.s.	n.s.	n.s.	n.s.	n.s.	*
Cpt-NC200 Irinotecan	n.s.	n.s.	n.s.	**	***	***
Cpt-NC50 Irinotecan	n.s.	*	n.s.	n.s.	n.s.	n.s.
Cpt-NC20 Irinotecan	n.s.	n.s.	n.s.	n.s.	n.s.	***

Fig. S8. Long-term antitumor efficacy study in athymic nude mice bearing subcutaneously implanted MCF-7 tumors. (*A*) Schematic illustration of the time line of the long-term efficacy study. (*B*) Injection protocol of all the treatment groups. [a] Administration schedules are abbreviated as follows: Q4d × 3, three injections with 4 day intervals; Qwk × 3, three injections with a 1 week interval. The first dose was administered on day 0 for all groups; [b] Each mouse was euthanized when the tumor size reached the end point (400 mg) or at day 60. N_{TR} =

Treatment Related Death; [c] N_{NTR} = Non Treatment Related Death; [d] N_{EU} is the number of mice euthanized after the end point of tumor size had been reached. (*C*) Statistical analysis of the tumor sizes. All the data were analyzed using one-way ANOVA (OriginPro) with post hoc Fisher's LSD test. Statistical *p*-value between two treatment groups for each measurement was calculated. The first column lists every two treatment groups to be compared. If the overall F ratio was significant, the means of different treatment groups were compared using Fisher's LSD test. The results were deemed significant at $0.01 < p < 0.05$, denoted as *; highly significant at $0.001 < p \leq 0.01$, denoted as **; extremely significant at $p \leq 0.001$, denoted as ***; and not significant at $p \geqslant 00.05$, denoted as n.s..

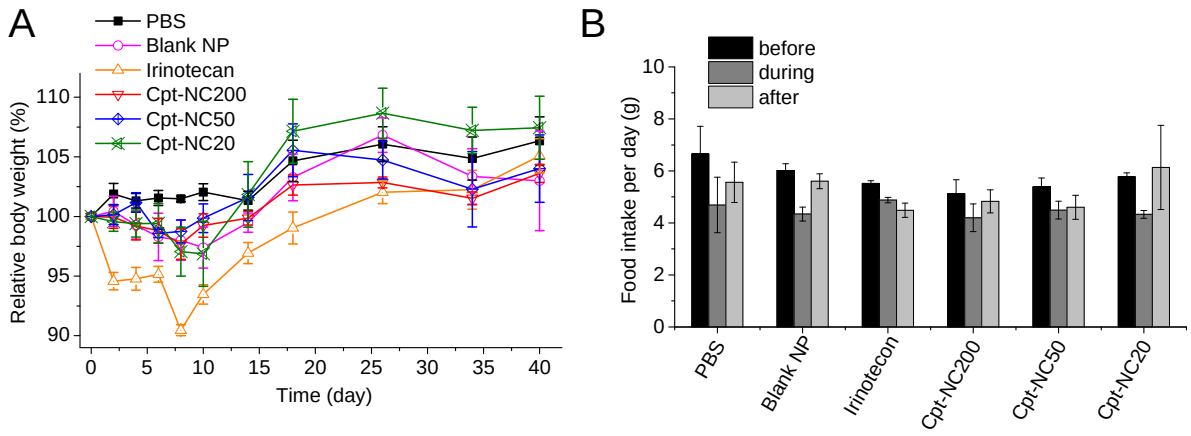

Fig. S9. Monitoring of body weight and food intake of athymic nude mice. (*A*) The body weight of mice were monitored during the whole study to evaluate if any acute toxicity caused by the treatment. Data are presented as average ± SEM. (*B*) Food intake of the mice per day in the efficacy study. The 24-h food intake was determined by measured the weight change of food and monitored three times (before, during and after the administration of drugs). Data are presented as average ± SEM.

In vivo efficacy studies in a metastatic tumor model.

In vivo lung tumor metastasis prevention and inhibition study in 4T1 murine breast cancer model. Female BALB/c mice (8 week old) received iv injection of luciferase-engineered 4T1 (1×10^5) cells via the lateral tail vein at Day 0, and then were randomized into 5 groups with 9-12 mice per group (Fig. S10*A*). The mice were treated three times (every four days) started from Day 1 by iv injection of PBS (1×), Cpt-NC200 (20 mg Cpt/kg), Cpt-NC50 (20 mg Cpt/kg), Cpt-NC20 (20 mg Cpt/kg) and ip injection of free irinotecan (20 mg/kg). The injection protocol is summarized in Fig. S10*B*. Food intake and body weight was measured every 4 days (Fig. S13*A* and *B*). The study was terminated at Day 14 and internal organs were collected at necropsy for evaluation.

During the course of study, tumor metastatic progression in lungs was closed monitored using a bioluminescence (BL) imaging system (Stanford Photonics, Palo Alto, CA, USA) with a dual micro-channel plate ICCD camera. BL imaging was conducted every 4 days to monitor the progression of metastasis induced by luciferase-engineered 4T1 cells. Each mouse was ip injected with D-luciferin potassium (0.15 g/kg body weight) 3 minutes prior to imaging, and then anesthetized with isoflurane/oxygen. A grey-scale image of the mouse was first recorded with dimmed light. Photon emission was then integrated for 3 minutes using the imaging software Piper Control (Stanford Photonics, Palo Alto, CA, USA) and visualized in pseudo-color. To localize BL signals that indicated luciferase-engineered 4T1 tumors, grey-scale images of mouse body and BL signals of metastatic tumors were merged using ImageJ (NIH). BL signals were semi-quantified by measuring the integrated density in the area shaped around each site of photon emission using ImageJ. The threshold for measurement was set as 5,000 empirically.

Scoring of metastases and histology analysis. At necropsy, internal organs including heart, lungs, kidneys, livers, spleens and intestines were excised and fixed in 10% formalin. Metastatic 4T1 tumors on the lungs were evaluated by two methods: counting the number of tumor nodules and scaling the severity of the tumor spreading on the surface of the lungs. In the former method, metastatic 4T1 tumor nodules on the lungs were counted with the aid of a dissecting microscope. In the latter method, metastatic 4T1 tumor spreading on the lungs was evaluated as following: lungs with over 90% surface occupied by tumors were scored as 5; 70-90% were as 4; 50-70%

were scored as 3; 30-50% were scored as 2; lungs with less than 30% surface occupied by tumors were scored as 1. In the present study, lungs with scale 1 were outliers, thus being excluded from analysis. Macro-metastatic tumors on organs other than the lungs were scarce. Internal organs including lungs, heart, livers, spleens, kidneys and intestines were embedded in paraffin, sliced into 5 μm and stained with hematoxylin and eosin (H&E) for histology analysis. Representative images were taken with an AxioSkop 40 microscope for all the tissues sections. All the data were analyzed using one-way ANOVA (OriginPro) with post hoc Fisher's LSD test.

In vivo biodistribution study in BALB/c mice bearing 4T1 metastatic tumors in lungs. Female BALB/c mice with metastatic 4T1 tumors in lungs (Day 10 post the iv injection of 4T1 cells) were divided into groups of five. Mice were injected iv with ^{64}Cu-NC200, ^{64}Cu-NC50 and ^{64}Cu-NC20 respectively (~50 μCi per mouse). Normal BALB/c mice without tumors were injected with ^{64}Cu-NC50 as a control. Mouse organs: heart, lung (with metastatic tumors), liver, spleen, and kidneys were harvested 24 h p.i.. The radioactivity of tissues was assayed by a γ-counter. To determine 100% dose, diluted solution of the corresponding ^{64}Cu-NCs was measured along with tissues at the same instrument settings. Data are presented as %I.D./g (average ± SEM). The statistical analysis was performed using a two-tailed Student's t-test, and p-values < 0.05 were considered statistically significant.

In vivo tumor penetration study in BALB/c mice bearing 4T1 metastatic tumors in lungs. Female BALB/c mice with metastatic 4T1 tumors in lungs (Day 10 post the iv injection of 4T1 cells) were divided into groups of three. Mice were injected iv with PBS or Rhd-NC200, Rhd-NC50 and Rhd-NC20 (200 μL, 15 mg/mL). The animals were euthanized 24 h after administration. The lungs were collected and immediately frozen in OCT and processed and stained similar as above mentioned. Fluorescence images were taken on a Zeiss LSM 700 confocal microscope.

A

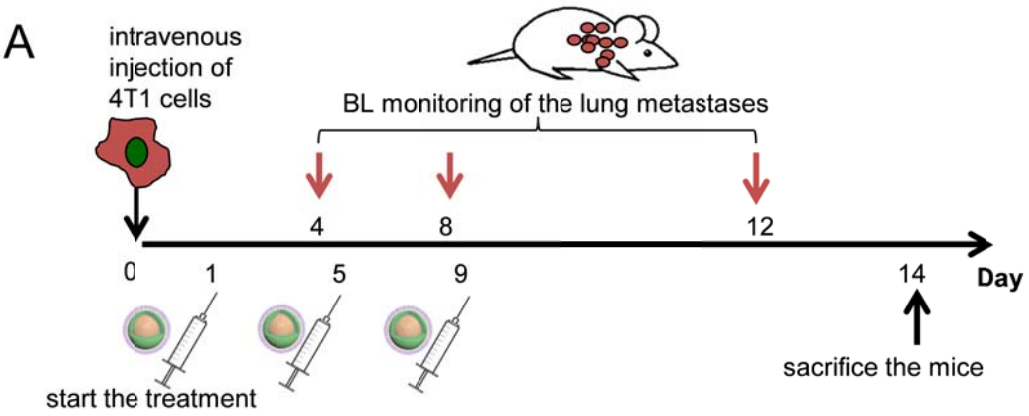

B

Group	Group description	No. of mice	Dose of drug equiv.	Injection route	Schedule
1	PBS	9	0	iv	Q4d × 3
2	Irinotecan	9	20 mg/kg	ip	Q4d × 3
3	Cpt-NC200	9	20 mg/kg	iv	Q4d × 3
4	Cpt-NC50	7	20 mg/kg	iv	Q4d × 3
5	Cpt-NC20	9	20 mg/kg	iv	Q4d × 3

Fig. S10. *In vivo lung* cancer metastasis prevention and inhibition study in 4T1 murine breast tumor model. (*A*) Schematic illustration of the time line of the efficacy study. (*B*) Injection protocol of all the treatment groups.

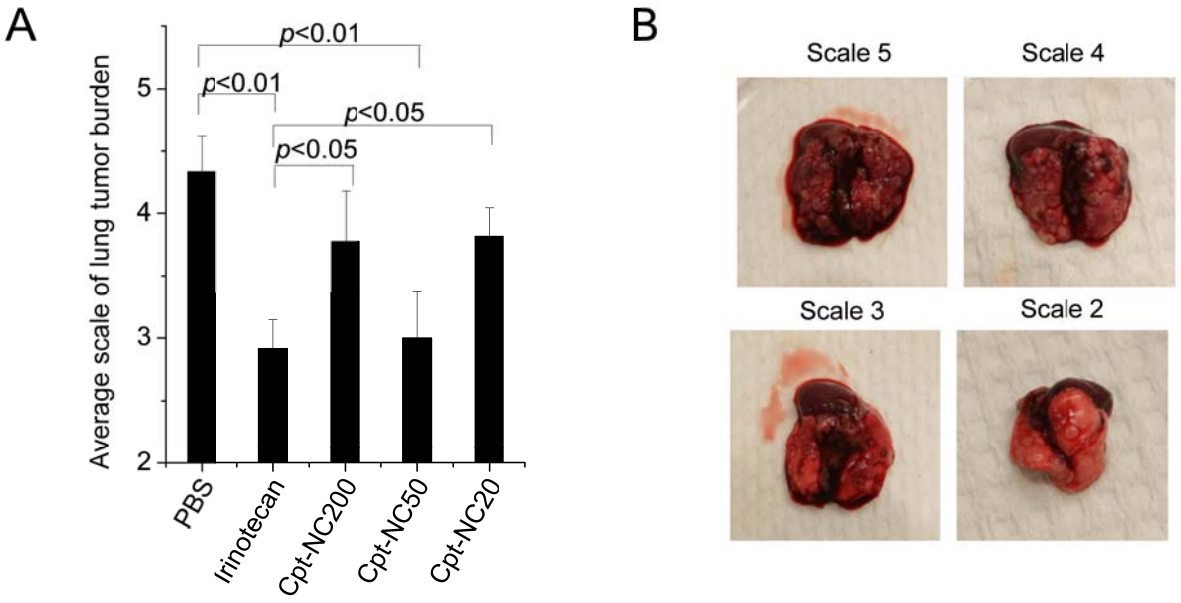

Fig. S11. Scaling of the lung tissues with metastatic tumors. (*A*) Lungs were excised at necropsy and scaled based on the severity of tumor spread on the lung surface. Lungs with over 90% surface occupied by tumors scored 5; lungs with 70-90% surface occupied by tumors scored 4; lungs with 50-70% surface occupied by tumors scored 3; lungs with 30-50% surface occupied by tumors scored 2; lungs with less than 30% surface occupied by tumors scored 1. In the present study, lungs with scale 1 were outliers, thus being excluded from analysis. Data are presented as average ± SEM and analyzed using one way ANOVA. (*B*) Representative lung pictures with scale 5, 4, 3 and 2.

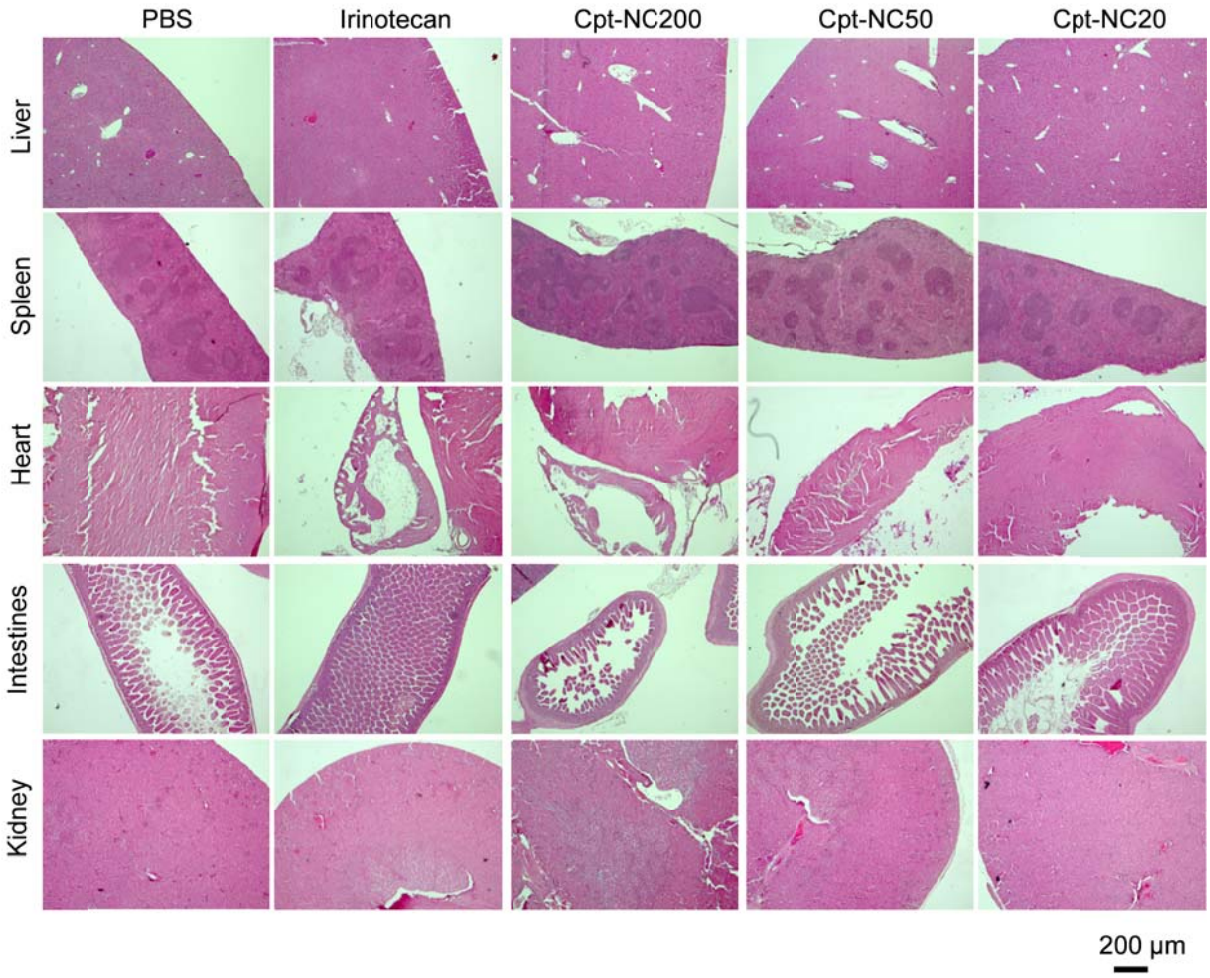

Fig. S12. Histopathology of tissues of BALB/c mouse. Internal organs, including heart, liver, kidney, spleen and intestine, were excised at necropsy and fixed in 10% formalin. Fixed tissues were embedded in paraffin and sectioned into 5 μm and stained with hematoxylin and eosin. Sectioned tissues were observed under a microscope with 50 × magnification, scale bar: 200 μm.

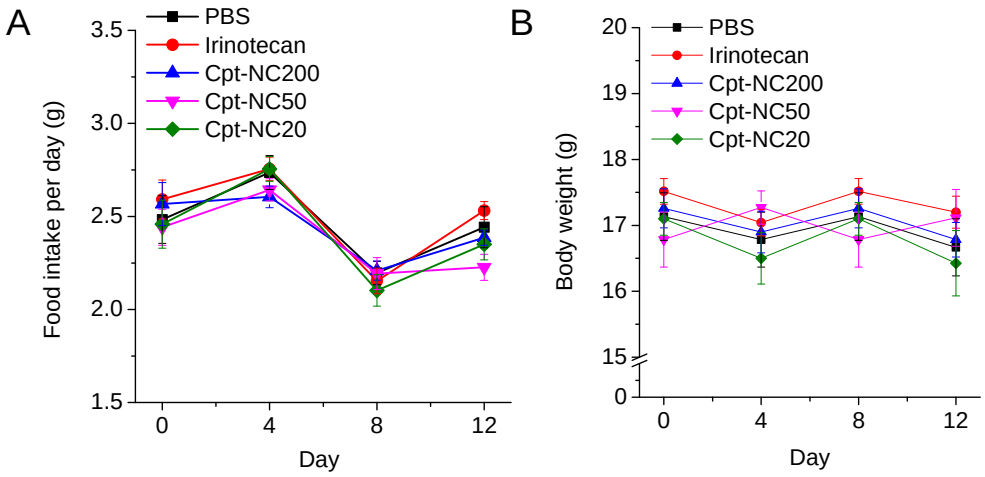

Fig. S13. Monitoring of body weight and food intake of BALB/c mice. (*A*) Food intake per day was measured every four days. (*B*) Body weight was measured every 4 days. Data are presented as average ± SEM.

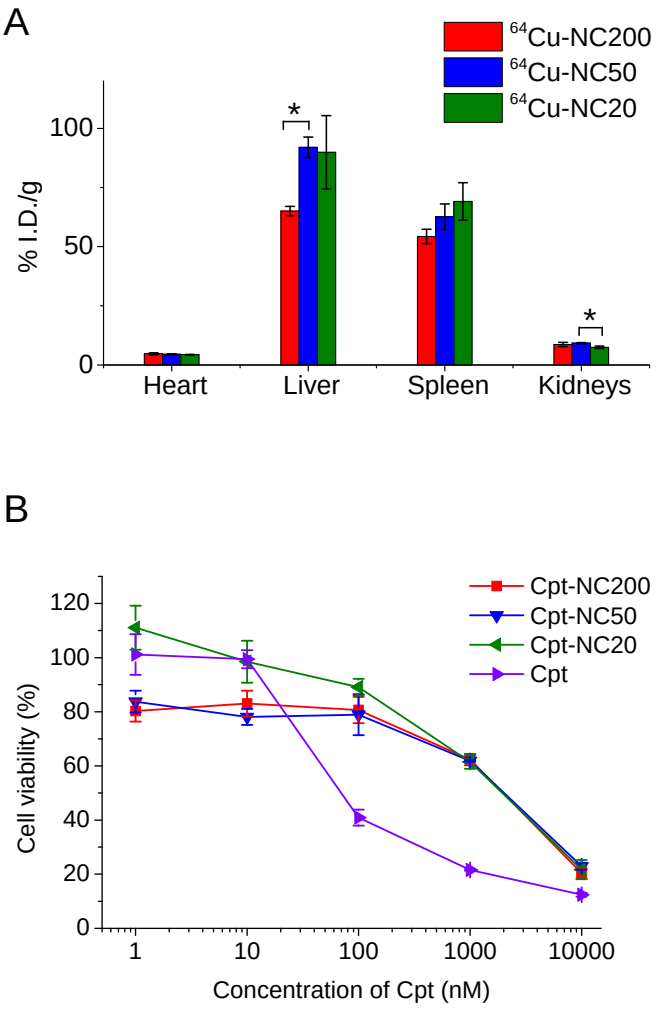

Fig. S14. (*A*) *In vivo* biodistribution studies in BALB/c mice bearing 4T1 metastatic lung tumors. BALB/c mice 4T1 metastatic lung tumors were injected iv with ^{64}Cu-NC200, ^{64}Cu-NC50 and ^{64}Cu-NC20 respectively (~50 μCi per mouse). Mice were euthanized 24 h p.i.. Mouse organs were collected and measured for radioactivity by γ-counter (average ± SEM; n = 5; two-tailed Student's t-test: *$p < 0.05$). (*B*) *In vitro* cytotoxicity of Cpt-NCs against 4T1 cells.

Spatio-temporal modelling of NP uptake into tumors

Spatio-temporal model. Using a similar approach to previous studies (7-10), we modelled the diffusion, cell surface association and dissociation, and cell internalization and externalization of NPs in an idealized spherically symmetric tumor by a set of coupled partial differential equations (Eqns. 1A-D),

$$\begin{aligned}
\frac{\partial C}{\partial t} &= \frac{1}{r^2}\frac{\partial}{\partial r}\left[D\epsilon r^2 \frac{\partial}{\partial r}\left(\frac{C}{\epsilon}\right)\right] - k_a C_{bs}\frac{C}{\epsilon} + k_d C_b \\
\frac{\partial C_b}{\partial t} &= k_a C_{bs}\frac{C}{\epsilon} - k_d C_b - k_i C_b + k_o C_i \\
\frac{\partial C_{bs}}{\partial t} &= -k_a C_{bs}\frac{C}{\epsilon} + k_d C_b + k_i C_b - k_o C_i \\
\frac{\partial C_i}{\partial t} &= k_i C_b - k_o C_i
\end{aligned} \tag{1A-D}$$

where C is the molar concentration of free NPs within the tumor volume, C_b is the molar concentration of NPs bound to the surface of tumor cells, C_{bs} is the molar concentration of NP binding sites on the surface of the tumor cells, and C_i is the molar concentration of internalized NPs within the tumor cells. The parameter t stands for time, and r for the radial distance from the center of the spherical tumor (r=0 is the origin of the spherical coordinate system located at the center of the tumor), D is the effective diffusion coefficient of the NPs within the tumor, and ε is the volumetric porosity of the tumor describing the fraction of the tumor volume that is available to free NPs. The parameter k_a is the rate constant for association of NPs and cell surface binding sites, k_d is the rate constant for the dissociation of NPs from the cell surface, k_i is the rate constant for the internalization of surface bound NPs into the cell, and k_o is the rate constant for the externalization of internalized NPs to the cell surface.

The initial conditions for these coupled equations are given by Eqns. 2A-B, reflecting the absence of any NPs within the tumor at t=0.

$$\begin{aligned}
C(t=0,r) = C_b(t=0,r) = C_i(t=0,r) &= 0, && 0 \le r \le R \\
C_{bs}(t=0,r) &= C_{bs}^0, && 0 \le r \le R
\end{aligned} \tag{2A-B}$$

where R is the radius of the spherical tumor, and C_{bs}^{0} denotes the total molar concentration of cell surface binding sites.

The boundary conditions for the system of equations are given by Eqns. 3A-B,

$$\frac{\partial}{\partial r}\left(\frac{C}{\epsilon}\right)(t, r=0) = 0$$
$$C(t, r=R) = \epsilon(r=R) C_{bulk}(t) \qquad \text{(3A-B)}$$

where $C_{bulk}(t)$ represents the time dependent molar concentration of free NPs at the tumor periphery. Eqn. 3A is a no flux condition at the center of the tumor that is a direct consequence of our imposition of spherical symmetry. Eqn. 3B describes the molar concentration of free NPs at the tumor periphery accounting for the reduced volume available to free NPs within the tumor relative to its surroundings.

We simplify our model by assuming the porosity, ε, and diffusivity, D, to be constant throughout the tumor, and therefore possess no radial dependence. Additionally, we set $C_{bulk}(t) = C_{bulk}^{0} \exp(-\lambda t)$, where C_{bulk}^{0} is the initial molar concentration of free NPs at the tumor periphery at t=0, and λ is the rate constant parameterizing the exponential decay of the free NP concentration outside the tumor. This function describes the first order decay of a δ-function pulse of NPs delivered into the tumor environment at t=0, where λ is specified by the clearance rate of NPs from the bloodstream.

Solution procedure. To solve the model described by Eqns. 1-3, we used the Method of Lines(11) to replace the spatial derivatives with finite difference approximations, transforming the system of coupled partial differential equations with derivatives in r and t to an initial value problem comprising system of coupled ordinary differential equations with derivatives in t alone. We solved this initial value problem using the ode15s numerical integrator in MATLAB R2012a (The Math Works, Natick, MA).

Model parameters. To fully specify our model, we require values for the 9 parameters ε, D, C_{bulk}^{0}, λ, C_{bs}^{0}, k_a, k_d, k_i and k_o. In the following bullet points we describe how we specified these values for three NPs diameters d_{NP} = 20, 50 and 200 nm by fitting to experimental data. The inferred parameter values are listed in Table S1.

- C_{bulk}^{0} was specified to match the experimental initial mass concentration of NPs in the blood of 1 mg/ml for all three NP diameters considered (d_{NP} = 20, 50 and 200 nm) assuming the dose is 1 mg NP per mouse and total blood volume is ~1 mL. We calculated the corresponding molar concentration assuming the NPs to be monodisperse spheres with a mass density of pure silica (ρ_{silica} = 2650 kg/m^3), resulting in C_{bulk}^{0}(20nm) = 1.50×10^{-1} μM, C_{bulk}^{0}(50nm) = 9.58×10^{-3} μM, and C_{bulk}^{0}(200nm) = 1.50×10^{-4} μM.

- We fixed $\lambda = \ln(2)/\tau_{1/2}$ to match the experimentally observed circulation half-life of silica NCs, $\tau_{1/2}$ = 3 h, which was approximately independent of NP diameter for the three NP diameters considered (d_{NP} = 20, 50 and 200 nm; Table 1).

- The tumor porosity was set to ε = 0.09, adopting the value computed by image analysis of a U87-MG glioma by Waite and Roth (10). In Fig. S18 we demonstrate that while the absolute mass of internalized NPs within the tumor predicted by our model depends on the precise value of this parameter, the trend in the internalized mass as a function of NP diameter is insensitive to the tumor porosity over the range of ε = 0.05-0.75.

- The rate constants $\{k_a, k_d, k_i, k_o\}$ and the initial concentration of cell surface NP binding sites C_{bs}^{0} were inferred by numerical fitting of these parameters to reproduce experimentally observed uptake into HeLa cells of PEGylated silica NCs containing rhodamine B isothiocyanate fluorescent dye. HeLa cells were incubated with NCs of diameter 20, 50, and 200 nm at a mass concentration of 3 mg/ml, and fluorescence-activated flow cytometry (FACS) used to follow the uptake at 30, 60, and 90 min for the 200 nm particles, and 30, 60, 120, and 240 min for the 20 and 50 nm particles. We have previously reported the results for the 200 nm particles in Ref. (1), and full details of the experimental procedures can be found therein. Using an identical protocol, we collected new data over longer time windows for the two smaller NCs in order to observe the approach to the equilibrium plateau required for robust fitting of our model parameters. The measured fluorescence intensity was converted into a molar concentration by assuming the saturation intensity for the 20 nm NPs to correspond to 10 ng per 100,000 cells (1) and converting the other fluorescence values in direct proportion. The volume of a HeLa cell was taken as 2000 μm^3 (12), and the NCs assumed to be monodisperse spheres with a mass density equal to that of pure silica (ρ_{silica} = 2650 kg/m^3).

To compare the predictions of our model (Eqns. 1-3) to the experimental uptake kinetics, we modified the governing equations to reflect the fact that the HeLa cells are exposed directly to the bulk free NP concentration, rather than residing within a tumor mass. Accordingly, we solved a reduced model comprising a system of ordinary differential equations describing the time dependent surface association/dissociation and internalization/externalization of NPs for a single cell (Eqns. 4A-C, 5A-B),

$$\begin{aligned}\frac{dC_b}{dt} &= k_a C^0_{bulk} C_{bs} - k_d C_b - k_i C_b + k_o C_i \\ \frac{dC_{bs}}{dt} &= -k_a C^0_{bulk} C_{bs} + k_d C_b + k_i C_b - k_o C_i \\ \frac{dC_i}{dt} &= k_i C_b - k_o C_i\end{aligned} \tag{4A-C}$$

$$\begin{aligned}C_b(t=0) &= C_i(t=0) = 0 \\ C_{bs}(t=0) &= C^0_{bs}\end{aligned} \tag{5A-B}$$

Assuming that the experimental FACS measurements correspond to the combined fluorescence from both the surface bound, C_b, and internalized, C_i, NCs, we numerically optimized the values of $\{k_a, k_d, k_i, k_o, C_{bs}{}^0\}$ to fit the experimental data. Fitting was performed using a simplex search in this five-dimensional space in MATLAB R2012a (The Math Works, Natick, MA), where the objective function was minimization of the mean square error between the simulated and experimental predictions of $[C_b + C_i]$ averaged over all experimental time points. In Fig. S15*A-C*, we present the experimental single cell NC uptake kinetics for each of the three NC diameters (20, 50 and 200 nm) alongside the numerical results of our model. The best fit values are listed in Table S1.

- The NP diffusivity, D, was computed as $D = \kappa D_0$. D_0 is the Stokes-Einstein prediction of an idealized spherical NP in free solution (7),

$$D_0 = \frac{k_B T}{3\pi\mu d_{NP}} \tag{6}$$

where k_B is Boltzmann's constant, T = 313 K is the temperature, $\mu = 6.53\times10^{-4}$ Pa.s is the viscosity of water at 313 K, and d_{NP} is the NP diameter, and κ is an adjustable parameter. We fit the value of κ for each NP diameter (d_{NP} = 20, 50 and 200 nm) by comparing our model predictions to previously reported *in vitro* penetration depths of PEGylated silica NCs containing IR783 near-infrared dye into approximately spheroidal LLC tumors with radius, R = 3.5 mm, after 48 h of incubation in a cell medium containing a mass concentration of NPs of 3 mg/ml(1). The penetration depth was defined as the radial distance from the tumor edge at which the fluorescent intensity decayed to 5% of its peripheral value. The reported values for d_{NP} = 20, 50 and 200 nm particles were 1396, 660, and 88 μm, respectively (1). These values are in good accord with new experimental data reported herein for the penetration of rhodamine labelled silica NCs in an MCF-7 tumor of 1413, 947, and 112 μm, respectively (Fig. S4).

For each of the three NP diameters, we numerically solved the model described by Eqns. 1-3 over a 48 h time window using the experimental values for C_{bulk}^{0} and R, and setting λ = 0, reflecting a constant bulk concentration of NPs, $C_{bulk}(t) = C_{bulk}^{0}$. Adopting ε = 0.09 and the best fit values for $\{k_a, k_d, k_i, k_o, C_{bs}^{0}\}$ computed above, we computed from our model the penetration depth as the radial distance from the tumor periphery at which the combined mass concentration of free, bound, and internalized NPs, $[M + M_b + M_i]$, dropped to 5% of its peripheral value, and numerically fitted the value of κ to reproduce the observed penetration depth using a one-dimensional simplex search in MATLAB R2012a (The Math Works, Natick, MA). In Fig. S15*D-F*, we present the numerical profiles for M_{tot} at t = 48 h predicted by our model for each of the three particle diameters using the best-fit values of κ. These values are listed in Table S1.

Parameter interpolation. The model parameters fitted to experimental data for the three NP diameters d_{NP} = 20, 50 and 200 nm (Table S1), may be used to interpolate values for NPs with intermediate diameters by fitting regression models to the data. In Fig. S16 we plot $\{k_a, k_d, k_i, k_o\}$ vs. d_{NP}, C_{bs}^{0} vs. $1/d_{NP}^{2}$, and κ vs. $1/d_{NP}$. In all instances, the linear correlation measured by Pearson's correlation coefficient, ρ, is strong ($\rho \geqslant 0.990$), and significant ($p < 0.10$, two-tailed Student's t-test).

- In line with physical intuition, the concentration of cell surface binding sites is observed to scale in inverse proportion to the NP cross-sectional area, $A_X \propto d_{NP}^{2}$. In contrast, the linear

correlation of C_{bs}^{0} with d_{NP} is much weaker and does not reach significance – $\rho(C_{bs}^{0}, d_{NP}) = -0.66$ ($p = 0.54$) – and with $1/d_{NP}$ is strong, but not significant – $\rho(C_{bs}^{0}, 1/d_{NP}) = 0.96$ ($p = 0.19$).

- Similarly, the strong linear correlation of κ with $1/d_{NP}$ is identical to the functional dependence of D_0 upon d_{NP} (Eqn. 6). The linear correlation of κ with d_{NP} is weaker and does not reach significance – $\rho(\kappa, d_{NP}) = -0.78$ ($p = 0.43$).

Supported by the strong observed linear correlations, we constructed ordinary least squares linear regression models for each panel in Fig. S16, and used these models to interpolate parameter values for NP diameters in the range $20 \leqslant d_{NP} \leqslant 200$ nm.

Table S1. Parameter values used in spatio-temporal model defined in Eqns. 1-3.

d_{NP} / nm	20	50	200
C_{bulk}^{0} / mol/m^3	1.5×10^{-4}	9.6×10^{-6}	1.5×10^{-7}
λ / s^{-1}	6.4×10^{-5}	6.4×10^{-5}	6.4×10^{-5}
ε / -	0.09	0.09	0.09
k_a / m^3/mol.s	8.3	1.1×10^{2}	4.2×10^{2}
k_d / 1/s	8.6×10^{-5}	1.1×10^{-4}	5.6×10^{-4}
k_i / 1/s	5.3×10^{-7}	1.7×10^{-5}	8.3×10^{-4}
k_o / 1/s	1.4×10^{-3}	2.0×10^{-3}	1.4×10^{-2}
C_{bs}^{0} / mol/m^3	1.4×10^{-5}	7.0×10^{-7}	3.6×10^{-8}
κ / -	7.5×10^{-2}	1.7×10^{-2}	3.3×10^{-4}
D_0 / m^2/s	3.5×10^{-11}	1.4×10^{-11}	3.5×10^{-12}

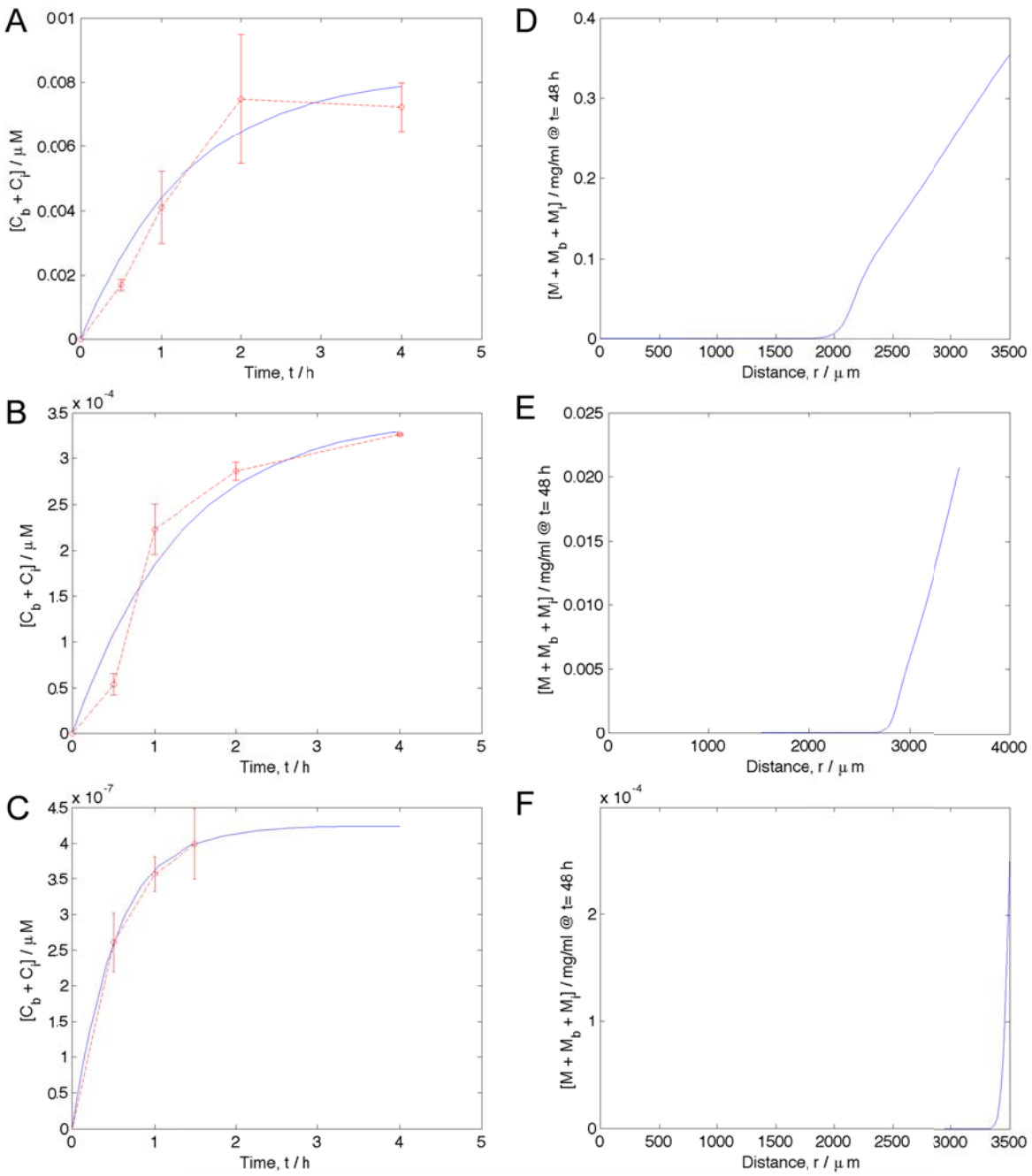

Fig. S15. Numerical fitting of model parameters $\{k_a, k_d, k_i, k_o, C_{bs}^0, \kappa\}$ to experimental data. Fitted parameter values are reported in Table S1. (*A-C*) The parameters $\{k_a, k_d, k_i, k_o, C_{bs}^0\}$ were adjusted for each NP diameter (*A*) d_{NP} = 20 nm, (*B*) d_{NP} = 50 nm, and (*C*) d_{NP} = 200 nm, by comparing the model predictions for the single cell NP uptake kinetics (Eqns. 4-5; blue solid lines) to experimental data (red dashed lines) for the uptake into HeLa cells of PEGylated silica

NCs containing rhodamine B isothiocyanate fluorescent dye (1). The experimental data collected over 90 min for d_{NP} = 200 nm in panel (*C*) is taken directly from Fig. 3*B* in Ref. [1]. The data in panels (*A*) and (*B*) for d_{NP} = 20 and 50 nm, respectively, collected over 240 min constitute new studies conducted as part of the present work following an identical experimental protocol to Ref. [1]. The values of $\{k_a, k_d, k_i, k_o, C_{bs}^{\,0}\}$ were numerically optimized for each particle diameter to minimize the mean squared error between the experimentally measured and model predictions for $[C_b + C_i]$. Error bars on the experimental data points represent the standard deviations computed from conducting each measurement in triplicate. (*D-F*) Having fitted $\{k_a, k_d, k_i, k_o, C_{bs}^{\,0}\}$, the value of κ for each NP diameter were numerically adjusted to obtain the best fit of the model predictions for the penetration depth of NPs into a spherical tumor (Eqns. 1-3) to previously reported *in vitro* penetration depths of PEGylated silica NCs containing IR783 near-infrared dye into LLC tumors with radius, R = 3500 μm, after 48 h of incubation in a cell medium containing a mass concentration of NPs of 3 mg/ml (1). Defining the penetration depth as the depth at which the combined concentration of free, bound, and internalized NPs drops to 5% of its peripheral value, the radial concentration profiles of $[M + M_b + M_i]$ at t = 48 h predicted by our model using the best fit values of κ for (*A*) d_{NP} = 20 nm, (*B*) d_{NP} = 50 nm, and (*C*) d_{NP} = 200 nm, exhibit penetration depths of 1400, 665, and 87.5 μm, respectively, in excellent accord with the previous experimental values of 1396, 660, and 88 μm (1).

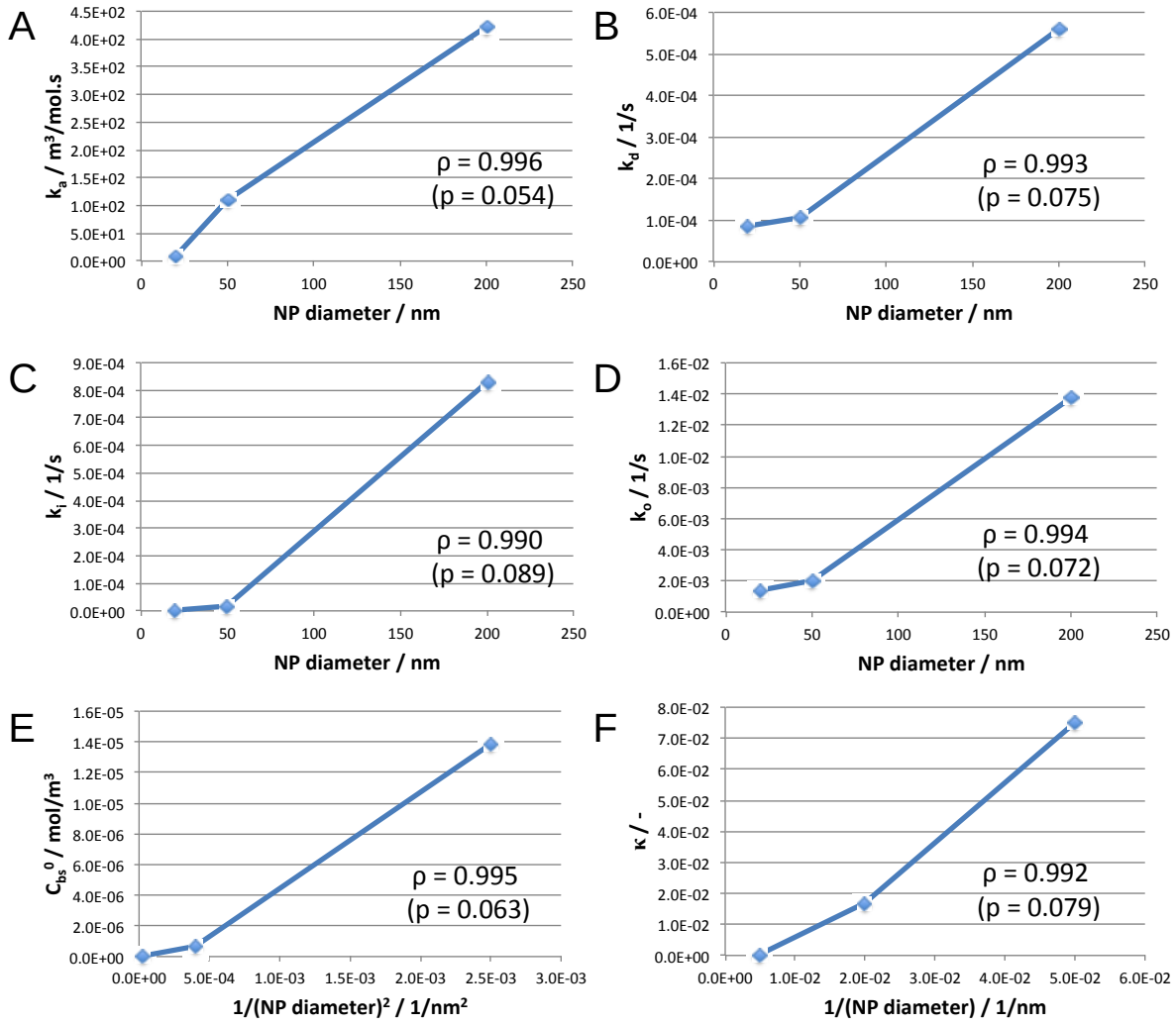

Fig. S16. Model parameter dependence on NP diameter, d_{NP}. Association rate constant, k_a (*A*), dissociation rate constant, k_d (*B*), internalization rate constant, k_i (*C*), externalization rate constant, k_o (*D*), total concentration of cell surface NP binding sites $C_{bs}^{\,0}$ (E), and empirical prefactor correction to Stokes-Einstein prediction of NP diffusivity, κ (*F*). In each panel we report Pearson's correlation coefficient as a measure of the strength of the linear correlation, and the associated p-value calculated from a two-tailed Student's t-test. In all cases the linear correlation is strong ($\rho \geqslant 0.990$), and significant ($p < 0.10$).

Statistical analyses

The statistical analysis was performed by one-way analysis of variance (ANOVA) (OriginPro) with post hoc Fisher's LSD test or a two-tailed Student's t-test, and *p*-values < 0.05 were considered statistically significant. The results were deemed significant at $0.01 < *p \leq 0.05$, highly significant at $0.001 < **p \leq 0.01$, and extremely significant at $***p \leq 0.001$.

References

1. Tang L, Fan TM, Borst LB, Cheng J (2012) Synthesis and Biological Response of Size-Specific, Monodisperse Drug–Silica Nanoconjugates. *ACS Nano* 6(5):3954-3966.
2. Stober W, Fink A, Bohn E (1968) Controlled Growth of Monodisperse Silica Spheres in Micron Size Range. *J Colloid Interface Sci* 26(1):62-69.
3. Tang L, et al. (2012) Aptamer-Functionalized, Ultra-Small, Monodisperse Silica Nanoconjugates for Targeted Dual-Modal Imaging of Lymph Nodes with Metastatic Tumors. *Angew Chem, Int Ed* 51(51):12721-12726.
4. Cabral H, et al. (2011) Accumulation of sub-100 nm polymeric micelles in poorly permeable tumours depends on size. *Nat Nanotechnol* 6(12):815-823.
5. Martin-Kleiner I, Svoboda-Beusan I, Gabrilovac J (2006) PMA and doxorubicin decrease viability, MTT activity and expression of CD10 marker on NALM-1 leukemic cells. *Immunopharmacol Immunotoxicol* 28(3):411-420.
6. Cheng J, Khin KT, Davis ME (2004) Antitumor activity of beta-cyclodextrin polymer - Camptothecin conjugates. *Mol Pharm* 1(3):183-193.
7. Goodman TT, Chen J, Matveev K, Pun SH (2008) Spatio-temporal modeling of nanoparticle delivery to multicellular tumor spheroids. *Biotechnol Bioeng* 101(2):388-399.
8. Graff CP, Wittrup KD (2003) Theoretical analysis of antibody targeting of tumor spheroids: Importance of dosage for penetration, and affinity for retention. *Cancer Res* 63(6):1288-1296.

9. Vanosdol W, Fujimori K, Weinstein JN (1991) An Analysis of Monoclonal-Antibody Distribution in Microscopic Tumor Nodules - Consequences of a Binding-Site Barrier. *Cancer Res* 51(18):4776-4784.
10. Waite CL, Roth CM (2011) Binding and Transport of PAMAM-RGD in a Tumor Spheroid Model: The Effect of RGD Targeting Ligand Density. *Biotechnol Bioeng* 108(12):2999-3008.
11. Schiesser WE, Griffiths GW (2009) A Compendium of Partial Differential Equation Models Method of Lines Analysis with Matlab Preface. *Compendium of Partial Differential Equation Models: Method of Lines Analysis with Matlab*:Ix-Xiii.
12. Zhao L, et al. (2008) Intracellular water-specific MR of microbead-adherent cells: the HeLa cell intracellular water exchange lifetime. *NMR Biomed* 21(2):159-164.